



Research Paper / Makale

Prediction of Muon Energy using Deep Neural Network
with Multiple Coulomb Scattering Data

Güral AYDIN^{1a}

¹Physics Department, Hatay Mustafa Kemal University, Hatay, Türkiye
gaydin@mku.edu.tr

Received/Geliş: 02.11.2021

Accepted/Kabul: 06.06.2022

Abstract: This study is based on determining muon beam energies using multiple Coulomb scattering data in artificial neural networks. Muon particles were scattered off a 50-layer lead object by using the G4beamline simulation program which is based on Geant4. Before working with deep neural networks, average scattering angle distributions regarding the number of crossed layers were analyzed with the fit method using the well-known formula for multiple Coulomb scattering to estimate muon beam energies. Subsequently, average scattering angles over the number of crossed layers from 1 to 10 were used in deep neural network structures to estimate the muon beam energy. It has been observed that deep neural networks significantly improve the resolutions compared to the ones obtained with the fit method.

Keywords: Unfolding momentum spectrum, muon beam, multiple Coulomb scattering, deep neural network

Çoklu Coulomb Saçılma Verileri ile Derin Sinir Ağlarını
Kullanarak Müon Enerjisinin Tahmin Edilmesi

Öz: Bu çalışma, yapay sinir ağlarında çoklu Coulomb saçılma verileri kullanılarak müon ışını enerjilerinin belirlenmesine dayanmaktadır. Müon parçacıkları, Geant4 tabanlı G4beamline benzetim programı kullanılarak 50 katmanlı bir kurşun nesneden saçıldı. Derin sinir ağları ile çalışmadan önce, katman sayısı cinsinden ortalama saçılma açısı dağılımları, müon ışını enerjilerini tahmin etmek için çoklu Coulomb saçılımı için iyi bilinen formül kullanılarak fit yöntemiyle analiz edildi. Daha sonra, müon ışını enerjisini tahmin etmek için derin sinir ağı yapılarında 1'den 10'a kadar katman sayısı üzerinden ortalama saçılma açıları kullanıldı. Derin sinir ağlarının, fit yöntemine göre çözünürlükleri önemli ölçüde iyileştirdiği gözlemlenmiştir.

Anahtar Kelimeler: momentum spektrumu çözülmesi, müon ışını, çoklu Coulomb saçılması, derin sinir ağı

1. Introduction

Charged particles are deflected as they pass an object. Most of these deviations are due to Coulomb scattering from the nuclei. These many small-angle deflections are called multiple Coulomb scatterings (MCS). The deviation in scattering angles due to MCS induces a Gaussian distribution in a plane and the width of the distribution can be approximated by Equation 1 [1]:

$$\sigma_0 \approx \frac{13.6 \text{ MeV}}{\beta c p} \sqrt{\frac{x}{X_0}} \left[1 + 0.038 \ln \left(\frac{x}{X_0} \right) \right] \quad (1)$$

where, βc is the velocity of the muons, x is the material thickness, X_0 is the radiation length of the material, p is the momentum of the muons, and c is the speed of the light. The width could be related

How to cite this article

Aydın G., "Prediction of Muon Energy using Deep Neural Network with Multiple Coulomb Scattering Data", El-Cezeri Journal of Science and Engineering, 2022, 9 (3); 975-987.

Bu makaleye atıf yapmak için

Aydın G., "Çoklu Coulomb Saçılma Verileri ile Derin Sinir Ağlarını Kullanarak Müon Enerjisinin Tahmin Edilmesi", El-Cezeri Fen ve Mühendislik Dergisi, 2022, 9 (3); 975-987.

ORCID: *0000-0002-4996-1174

to the space angle approximately as given with Equation 2.

$$\sigma_0 = \sigma_{plane} = \frac{1}{\sqrt{2}} \sigma_{space} \quad (2)$$

The radiation length is then given as follows with Equation 3:

$$X_0 = \frac{716.4 \text{ g/cm}^2}{\rho} \frac{A}{Z(Z+1) \log(287/\sqrt{Z})} \quad (3)$$

Where Z is the atomic number, A is the atomic mass of the material, and ρ is the density of the material. For the same material and thickness, the scattering angle distribution will depend on the muon beam energies; with higher energy, muons will have a scatter distribution with smaller widths. One of the rapidly developing research topics is using these scattering angle data with appropriate techniques to determine the momentum of charged particles in the absence of a magnetic field. Another application area of the MCS is muon tomography. Muon tomography is based on the MCS of highly penetrating cosmic ray muon particles as they pass through the object to be detected [2, 3]. It has many applications for inspecting objects in volcanology, special nuclear materials, the shipping industry, and civil engineering. The main advantage of muon tomography is that it does not need unnatural radiation sources.

The MCS data can be used to determine charged particle momentum even in the absence of a magnetic field by using detectors that can measure particle trajectories with good precision. In other words, predicting the momentum of charged particles relies on precise measurements of particle scattering angles. Cloud chambers [4, 5], emulsion detectors [6], and spark chambers [7] are the early applications of this theory to measure charged particle momentum. MACRO collaboration [8, 9] used streamer tubes to measure the momentums of through-going atmospheric muons with MCS. On the other hand, the ICARUS collaboration [10] used T600 liquid argon (TPC) to measure the muon's momenta. If used as the target material, dense materials are also alternatives for measuring charged particle momenta [11, 12]. One of the techniques for measuring particle momentum is to scatter particles from an object in layers. In this case, dense absorbers and position-sensitive detectors are formed in layers and can be used to determine scattering angles in each layer. In this configuration, a cell is defined as a pair of absorbers and position-sensitive detectors [13]. The dependence of the average scattering angles in terms of the number of crossed cells can be used to determine the particle momentum with the help of the well-known MCS formula. This study aims to improve the energy resolutions of muon beams, which could be obtained with the fit method, by using the deep neural network structures which have received rising interest from scientists in recent years [14-22]. This work can also be evaluated as a study of how effective artificial neural networks can be in measuring the energies of charged particles through the geometries described in this paper.

Cosmic rays, primarily protons, constantly bombard the earth. These cosmic rays interact with the higher parts of the atmosphere, producing many short-lived secondary particles. Muons are produced as a result of the decay of these secondary particles. Muons can reach the earth's surface mainly because they interact with the Coulomb force, which accumulates energy in matter more slowly than the nuclear force. In horizontal detectors, the muon flux at sea level is approximately one muon / cm² / min [23]. Knowing the energies of cosmic ray muons is essential in several ways. For example, cosmic-ray muons could be used as a particle source to check and calibrate the detectors in nuclear and particle physics experiments. In some cases, it is essential to know the flux of the cosmic rays since they could be a background in a significant amount in an experiment. On the other hand, if the cosmic-ray data in some parts of the earth are evaluated with the primary cosmic-ray data, this could lead to understanding the cosmic-ray information at the upper cascade of the earth. The effect of the cosmic rays on human health is also under discussion by scientists. This study explores using neural

network structures to determine muon energy based on MCS with a setup of position-sensitive detectors and dense absorbers. Previous studies have shown that the muon tomography system can reach a spatial resolution of 50 μm with micro-pattern gas detectors or drift chambers and a few mm in a system formed with fibers embedded in plastic scintillators [24-28]. Another technique uses emulsion films for high-resolution particle tracking [13]. Therefore, these studies have shown the possibility of reconstructing particle trajectories with high precision resolutions. This work investigates ANN structures to precisely determine muon beam energy using scattering angles in a detector system with multiple absorber layers. This work is specific to muon particles, but it is essential to show how the algorithms presented can effectively determine the momentum of charged particles.

2. Material and Methods

In this section, the simulation program used in the study will be explained in the material subsection, and the methods used in the determination of muon energies will be explained under the title of the method.

2.1. Material

The simulation study was conducted with G4beamline [29] to obtain the scattering angle distributions of muons with different energies that strike the lead absorber vertically. This study used a geometry of successive layers of absorbers and position-sensitive plates. Fifty layers of scattering plates were constructed horizontally with the absorption material of lead having 200 cm x 200 cm transverse size and 1 mm thickness. In the simulated setup, position sensitive-detectors were placed before and after the absorbers to obtain particle information. Figure 1 shows the geometry of the detector design with 5 event display. G4beamline is based on the Geant4 toolkit [30-32], and it simulates particle transportation in the matter. It does not require complex programming to design detector geometries. Its other significant advantages are that it presents beam specifications, and beam track information can be output in several formats. It has a rich repository for beamline elements, and many beamline parameters can be tuned automatically. In G4beamline, the particle id, momentum, and position components of the particles hitting the detectors are saved with their event numbers in the related detector branch. This information was enough in our analysis to determine scattering angles at each layer without any uncertainty.

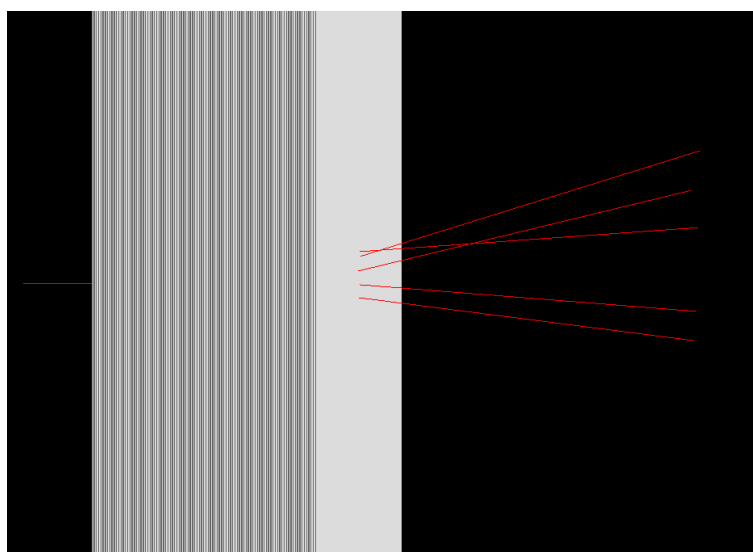


Figure 1. The detector geometry from the side view with 5 event display

2.2. Methods

This section explains two different methods to determine muon beam energies.

2.2.1. The Fit Method

One method that can be used to determine beam energy is to measure the average scattering angles as a function of the number of crossed cells. In this study, the space scattering angles have been determined at each layer by using the scalar product of the momentum vectors of the incoming and scattered muons. This momentum information was taken from the virtual detectors placed before and after the absorbers in the simulation program. In this way, the particle trajectories or directions are assumed to be determined without uncertainty. In an actual experiment, possible uncertainties could be considered by defining resolution parameters related to the angular resolution [13]. In an actual experiment, the effect of the scattering of the particles through the position-sensitive detectors could be considered negligible. Once the space angle was determined, the plane angle was obtained according to Equation 2. The average scattering angles for a certain number of crossed cells could be determined by taking account of various angle measurements over the corresponding number of absorbers. For example, considering two crossed cells, 49 measurements are possible with 50 absorber layers, and so on. The number of possible measurements in a given depth cell could be formulated with Equation 4 [13].

$$N_{meas} = \sum_{i=1}^{N_{cell}} int \left[\frac{N_{pl} - i + 1}{N_{cell}} \right] \tag{4}$$

Here N_{cell} refers to the number of crossed cells by a particle (depth of the cell), and N_{pl} is the number of absorber plates that a track could span.

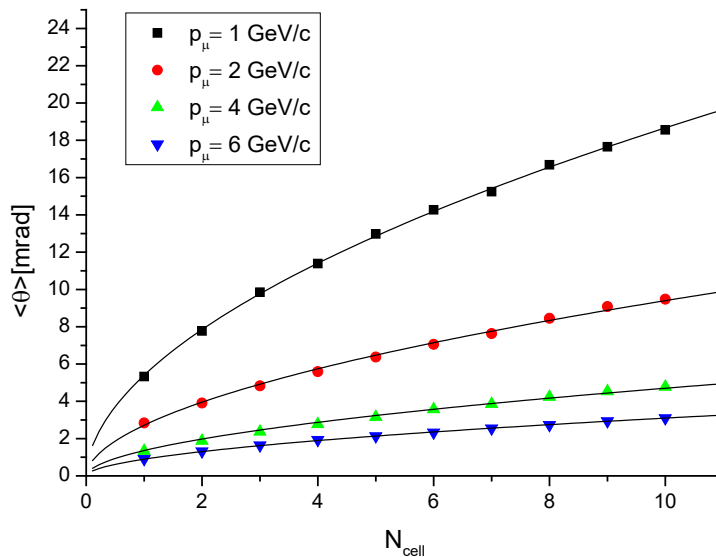


Figure 2. Average scattering angles as a function of the number of crossed cells for different muon beam energies. The solid lines are the fit functions given by Equation 5

The average scattering angles were determined based on the number of crossed cells. These angles could be fitted with Equation 5 to determine the particle momentum.

The absorber's length was taken as the number of crossed cells in the equation since we used 50 layers of absorber thickness of 1 mm. The beam momentum could be predicted in the numerical approach

by fitting the average scattering angle distributions with Equation 5 by defining momentum (p) as a free parameter. The fit example is shown in Figure 2 for various beam energies.

$$\sigma_0 \approx \frac{13.6 \text{ MeV}}{\beta c p} \sqrt{\frac{N_{cell}}{5.6}} \left[1 + 0.038 \ln \left(\frac{N_{cell}}{5.6} \right) \right] \quad (5)$$

In this approach, it is suitable to produce two different momentum distributions obtained with fit parameters to analyze momentum resolutions: distributions of fit momentum parameters (p) and inverse fit momentum parameters ($1/p$). Then, fitting those distributions with an appropriate function provided the momentum resolution with a specified resolution description. This study investigated the momentum resolutions with the fit method for the beam energies of 1 GeV, 2 GeV, 4 GeV, and 6 GeV. The reconstructed momentums (p_{recon}) were obtained with fit momentum parameters. Then, the momentum resolutions were obtained with two different distributions: One uses ($1/p_{recon}$) and the other takes only (p_{recon}). Both distributions were fit with the function of $f(A; mean; \sigma; \sigma r; \sigma l; const)$ given by Equation 6.

$$\begin{aligned} gaus &= A \exp \left(-0.5 \times \left(\frac{mean - x}{\sigma} \right)^2 \right) \\ expor &= A \exp \left(0.5 \times (\sigma r)^2 - \left(\frac{x - mean}{\sigma} \right) \times (\sigma r) \right) \\ expol &= A \exp \left(0.5 \times (\sigma l)^2 - \left(\frac{mean - x}{\sigma} \right) \times (\sigma l) \right) \\ rightCut &= mean + (\sigma) \times (\sigma r) ; \quad leftCut = mean - (\sigma) \times (\sigma l) \end{aligned} \quad (6)$$

$$f(A; mean; \sigma; \sigma r; \sigma l; const) = \begin{cases} gaus + const, & x < rightCut \text{ and } x > leftCut \\ expor + const, & x \geq rightCut \\ expol + const, & x \leq leftCut \end{cases}$$

Here (σr) and (σl) denote how many (σ) beyond the mean the right and left tails of the distribution begin, respectively. A refers to the amplitude of the function.

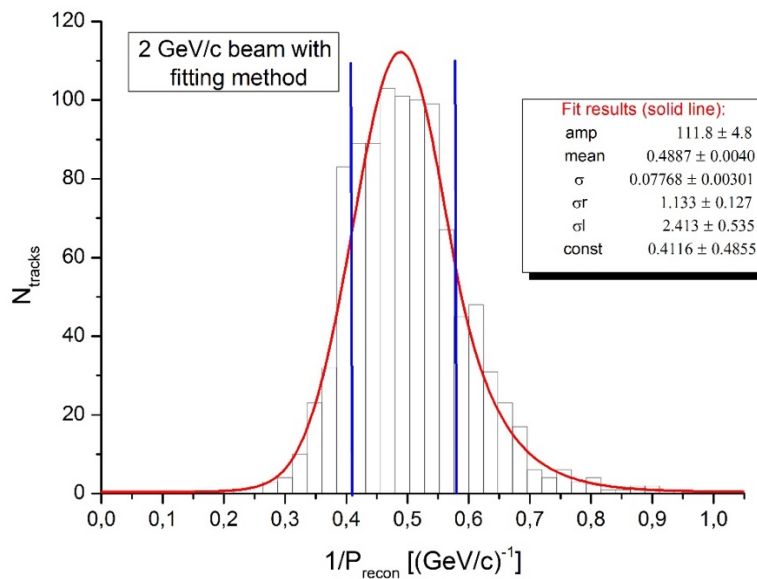


Figure 3. Inverse reconstructed momentum distributions of 2 GeV/c muon beam. The solid red line represents the fit function given by Equation 6. The blue lines correspond to the borders of the σ_{68} interval defined in the text.

This fit function is defined to be Gaussian with exponential tails. It was found that this function describes both momentum distributions quite well. The fit examples are shown in Figure 3 and Figure 4 for inverted and not inverted reconstructed momentum distributions, which belong to 2 GeV/c beams, respectively. The resolution was then determined using a 68% interval around the mean of the distribution. The interval covering 68% side area was determined with fit parameters on each side around the mean. Then, the half-width of the whole interval was defined to be σ_{68} and σ_{68}/p_{mean} was taken as the resolution value.

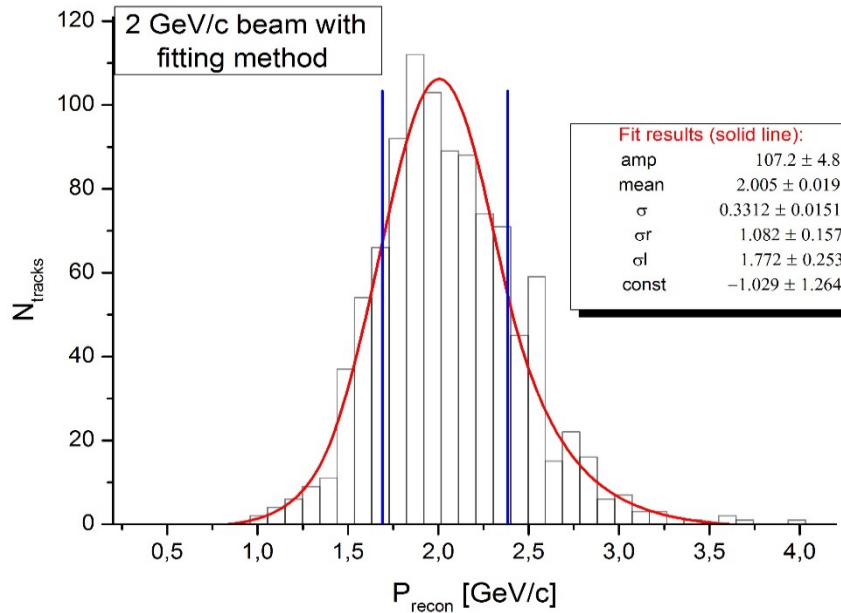


Figure 4. Reconstructed momentum distributions of 2 GeV/c muon beam. The solid red line represents the fit function given by Equation 6. The blue lines correspond to the borders of the σ_{68} interval defined in the text.

2.2.2. Deep Neural Network

Keras [33], written in Python, is a deep learning API (application programming interface). It runs on Tensorflow [34], an open-source machine learning platform that allows the development and trains machine learning models, instant model iteration, and easy debugging. The Keras contains essential abstractions and building blocks with high iteration velocity.

Layers and models are the main structures in Keras. The sequential model in Keras includes a linear stack of layers. The sequential model could be considered a functional API model in which each layer has input and output attributes. This study used the sequential model to define hidden layers, input shape, and output layer.

Keras has different activation functions: RELU, sigmoid, softmax, Softplus, Softsign, Tanh, Selu, Elu, and Exponential. Relu is the rectified linear unit activation function. The Relu activation function was used for the hidden layers in this study. This function is linear for positive input values and nonlinear for values less than 0. This activation function could be described mathematically as below with Equation 7 for the input value of z :

$$g(z) = \max(0, z) \quad (7)$$

The function does not require exponential computing, so it takes less computation time. The linearity of the function also eliminates the gradient vanishing effect caused by nonlinear functions [35].

On the other hand, the sigmoid function was used as the activation function between the last hidden layer and the output layer. This function returns the values between 0 and 1 and could be considered the 2-element softmax function, whose second element is 0. The sigmoid function is given by Equation 8.

$$\text{sigmoid}(x) = 1/(1 + \exp(-x)) \quad (8)$$

Adam (Adaptive Moment Estimation) is an optimization algorithm that uses the stochastic gradient descending (SGD) method. This method is efficient in the case of situations with extensive data and parameters [36]. It is stated that hyper-parameters need little tuning in the algorithm, which is also helpful for noisy problems and sparse gradients. SGD method is efficient in deep learning applications [37-41]. Adam takes advantage of two different methods: One is helpful for sparse gradients [42], and the other is efficient in online and non-stationary settings [43].

In the present study, binary cross-entropy class was used as the probabilistic losses where cross-entropy metrics are computed between the true and predicted labels. On the other hand, the argument "learning_rate" was used to determine the step size during the updating weights. This argument was set in the Adam optimization method. Metric is used to determine the level of the successfulness of a model. The main difference between the metrics and losses is that metrics are not used in the training process, while losses functions are used. In this study, an accuracy metric was used to evaluate the performance of the fit model. This metric compares the true and predicted labels and defines how often labels and predictions match. Input parameter set and true labels were scaled through "MinMaxScaler." This scaling is done so that the scaled data sets take values between 0 and 1. In this way, the predicted labels were then obtained for the values again between 0 and 1. The formula for scaling is given with Equation 9.

$$X_{norm} = \frac{X - \min(X)}{\max(X) - \min(X)} \quad (9)$$

Where X is the value to be normalized and $\min(X)$ and $\max(X)$ are the minimum and the maximum values in a given data set, respectively.

3. Results and Discussion

The resolution values obtained with the fitting method are shown in Table 1 for different beam energies. It is seen that the results are close to each other regarding beam energies, and they take the average values between 17% and 18%. The average values were obtained over two different fitting methods. The resolution errors were defined by taking the differences of the individual resolutions from the average resolution.

Table 1. Reconstructed momentum values vs. true momentum values. Average reconstructed momentums $\langle p \rangle$ and momentum resolutions $\langle \frac{\sigma_{68}}{p_{mean}} \rangle$ % are shown

p_{true} (GeV/c)	$\langle p \rangle$ (GeV/c)	$\langle \frac{\sigma_{68}}{p_{mean}} \rangle$ %
1	0.99 \mp 0.02	17.86 \mp 0.13
2	2.03 \mp 0.05	17.52 \mp 0.14
4	4.13 \mp 0.18	17.95 \mp 0.48
6	6.23 \mp 0.17	17.69 \mp 0.20

Error calculation related to the prediction of the true labels with deep learning structures was performed with the RMSE (Root Mean Squared Error) value. The formulation of such error is given with Equation 10.

$$rMSE = \sqrt{\frac{1}{N} \sum_{i=1}^N (x_i - y_i)^2} \quad (10)$$

where x_i is the predicted label value and y_i is the true label value for the i^{th} data.

The detector geometry used with ANN was the same as that used for the fitting procedure. This time, the muon beam energies were uniformly and randomly distributed in the simulation with 100000 muon particles. Half of this data was used for training purposes, and the remaining data were for the testing process. 30% of the data was left for validation purposes in the training process. The learning rate and batch size hyperparameters were optimized as 0.01 and 32, respectively. In the model, three different numbers of hidden layers (1, 2, and 3) and four different numbers of neurons (30, 60, 120, and 180) at each layer were set up and tested. Table 2 shows the configurations for each model. The RMSE values corresponding to each setup were obtained according to Equation 10 and are shown in Table 3. As it is shown, the best score was obtained through 3 layer configuration, each with 120 neurons. It is also seen that there is no significant difference between models in terms of RMSE values. Table 4 shows the hyperparameters which provide the best estimation. It was seen that there is no significant difference between validation and training loss during the training process.

Table 2. Deep learning models used for the estimation of muon momentums

	# of hidden layers	# of neurons at each layer
Model #1	1	30
Model #2	1	60
Model #3	1	120
Model #4	1	180
Model #5	2	30
Model #6	2	60
Model #7	2	120
Model #8	2	180
Model #9	3	30
Model #10	3	60
Model #11	3	120
Model #12	3	180

Table 3. Performance results of different deep learning models

	rMSE
Model #1	0.433549
Model #2	0.431063
Model #3	0.436451
Model #4	0.434121
Model #5	0.44378
Model #6	0.438078
Model #7	0.439559
Model #8	0.431312
Model #9	0.432711
Model #10	0.43679
Model #11	0.430044
Model #12	0.434951

Table 4. Parameters of the neural network model which leads to the best accuracy

Parameter	Value
Number of hidden layers	3
Number of neurons	120
Learning rate	0.01
Batch size	32
#epochs	100

Since beam momentum distribution is uniform for this study, the differences between expected and predicted momentum values were evaluated. The distributions of these differences were fitted again with Equation 6. Then, half-width at half maximum was determined through the σ_{68} parameter. These distribution plots were produced for the data around specific expected beam momentums to compare the results with the ones obtained with the fit method explained in Section 2. For example, the data around 2 GeV beam was taken as $1.95 \text{ GeV} < p < 2.05 \text{ GeV}$. Here, p is the expected (true) beam momentum. These difference distributions were also produced by the fit method for comparison. The fit examples are shown in Figure 5 and Figure 6 obtained with the ANN and the fit method for the beam around 1 GeV/c, respectively. Then, σ_{68} values were compared for two different methods. Table 5 shows the results, and it is seen that the results are significantly better with deep neural network structures than the ones with the fit method. Regarding two different σ_{68} values, the improvement with ANN was determined to be from 38% to 54%, considering the mentioned beam energies (1 to 6

GeV). For example, at $0.95 \text{ GeV} < p_{true} < 1.05 \text{ GeV}$, the σ_{68} value was 0.0889 GeV/c with the ANN method, while it was 0.1774 GeV/c with the fit method.

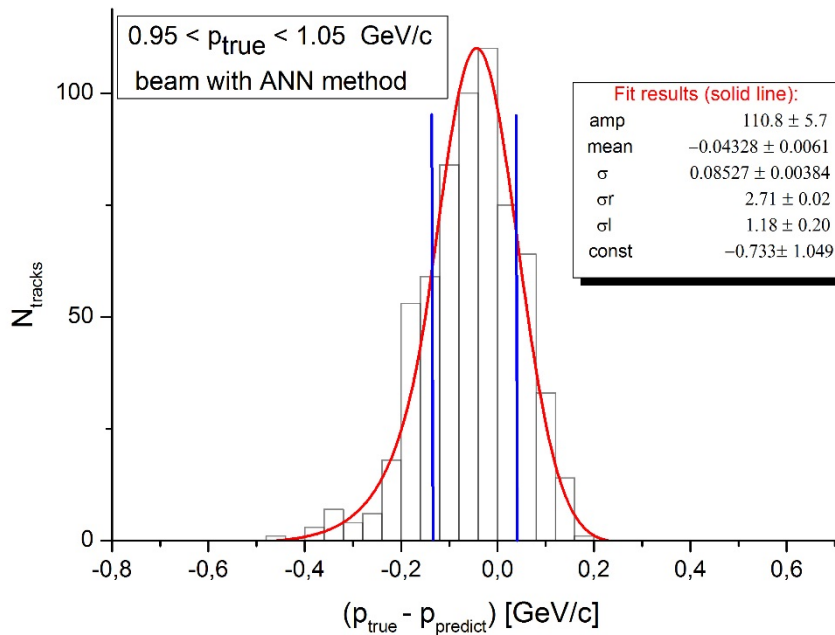


Figure 5. The differences between the true momentum values and the predicted ones were obtained with the ANN method. The solid red line represents the fit function given by Equation 6. The blue lines correspond to the borders of the σ_{68} interval in the fit function

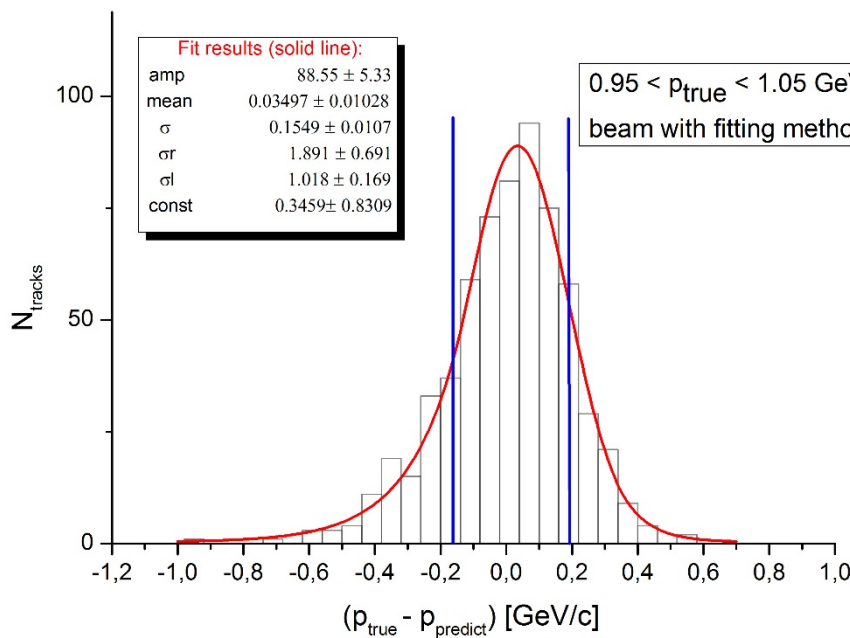


Figure 6. The differences between the true momentum values and the predicted ones were obtained with the fit method. The solid red line represents the fit function given by Equation 6. The blue lines correspond to the borders of the σ_{68} interval in the fit function

Table 5. Momentum resolutions with deep neural networks and comparison with the results obtained from the fit method

Momentum resolutions related to the distributions for the difference between expected (true) and predicted momentum values					
Momentum [GeV/c]	ANN		Fit method		Comparison $\Delta\sigma_{68}/\sigma_{68}(fit) \%$
	σ_{68}	p_{mean}	σ_{68}	p_{mean}	
$0.95 < p_{true} > 1.05$	0.0889	-0.0433	0.1774	0.0350	49.9
$1.95 < p_{true} > 2.05$	0.2012	-0.0829	0.3251	-0.0409	38.1
$3.95 < p_{true} > 4.05$	0.3538	0.0158	0.7721	-0.1287	54.2
$5.95 < p_{true} > 6.05$	0.5141	-0.3462	1.0463	-0.2587	50.9

4. Conclusions

Using simulation software to determine their energies, muons, vertically hitting a 1 mm thick 50 lead layers, were investigated through scattering angles. The aim was to use deep neural network structures to improve the energy resolutions obtained through numerical algorithms. The fit method takes account of average scattering angles in terms of the number of crossed cells by the incoming muon beam. This method was applied for the data, considering the configuration of 50 layers of lead absorbers. The average scattering angles were determined for the number of crossed cells from 1 to 10. Then, the obtained average angle distributions were fitted with the function of the well-known Coulomb scattering formula. The fit results provided the predicted momentum values, set as a free parameter in the fit function. Then, the momentum resolutions were obtained by fitting the distributions of the reconstructed momentums with an appropriate function. The fitting procedure was applied for the specific beam energies of 1, 2, 4, and 6 GeV/c muon beam, and it was seen that the resolutions are close to each other. The resolutions were around 17%, and it was found to be 17.5% for the beam momentum of 1 GeV/c. The related data were obtained with a muon beam whose energy is uniformly and randomly distributed to study momentum reconstruction with ANN. In total, 100000 events were constructed in the simulation program to be used with ANN structures. It was found that the momentum resolutions obtained with ANN are significantly better than the ones with the fit method. The improvements are achieved up to 54% considering the difference in σ_{68} values. The results show that deep neural network structures are worth using for the momentum reconstruction of cosmic ray muon beam or generally for charged beam momentum unfolding through scattering off dense objects in layers.

Authors' Contributions

GA carried out the study and wrote up the article. The author read and approved the final manuscript.

Competing Interests

The authors declare that they have no competing interests.

References

- [1]. Tao W.M. et al. (Particle Data Group), "Review of Particle Physics", J. Phys. G: Nuclear Part. Physics, 2006, 33(1):1-1232.

- [2]. Moliere G.V., "Theorie der Streuung schneller geladener Teilchen I", *Z. Naturforschg A*, 1947, 2a:133-145; Moliere G.V., "Theorie der Streuung schneller geladener Teilchen II", *Z. Naturforschg A*, 1948, 3a:78-97.
- [3]. Bethe H.A., "Molière's Theory of Multiple Scattering", *Phys. Rev.* 1953, 89:1256.
- [4]. Olbert S., "Application of the Multiple Scattering Theory to Cloud-Chamber Measurements I", *Phys. Rev.* 1952, 87:319.
- [5]. Annis M., Bridge H.S., Olbert S., "Application of the Multiple Scattering Theory to Cloud-Chamber Measurements II", *Phys. Rev.*, 1953, 89:1216.
- [6]. Voyvodic L., Pickup E., "Multiple Scattering of Fast Particles in Photographic Emulsions", *Phys. Rev.*, 1952, 85:91.
- [7]. Pinkau K., "Moliere's Theory of Multiple Scattering Applied to the Spark Chamber", *Z. Phys.*, 1966, 196(2):163-173.
- [8]. Ambrosio M., Antolini R., Auriemma G., Bakari D., Baldini A., Barbarino G.C. et al., "Muon energy estimate through multiple scattering with the MACRO detector", *Nuclear Instruments and Methods in Physics Research Section A*, 2002, 492(3): 376-386.
- [9]. Ambrosio M., Antolini R., Bakari D., Baldini A., Barbarino G.C., Barish B.C. et al., "Atmospheric neutrino oscillations from upward throughgoing muon multiple scattering in MACRO", *Phys. Lett. B*, 2003, 566(1-2): 35-44.
- [10]. Ankowski A., Antonello M., Aprili P., Arneodo F., Badertscher A., Baiboussinov B. et al., "Measurement of through-going particle momentum by means of multiple scattering with the ICARUS T600 TPC", *Eur. Phys. J C*, 2006, 48:667-676.
- [11]. Borozdin K.N., Hogan G.E., Morris C., Priedhorsky C., Saunders A., Schultz L.J. et al., "Radiographic imaging with cosmic-ray muons", *Nature*, 2003, 422: 277.
- [12]. Pesente S., Vanini S., Benettoni M., Bonomi G., Calvini P., Checchiha P. et al., "First results on material identification and imaging with a large-volume muon tomography prototype", *Nuclear Instruments and Methods in Physics Research Section A*, 2009, 604(3):738-746.
- [13]. Agafonova N., Aleksandrov A., Altinok O., Anokhina A., Aoki S., Ariga A. et al., "Momentum measurement by the multiple Coulomb scattering method in the OPERA lead-emulsion target", *New Journal of Physics*, 2012, 14:013026 (19 pp).
- [14]. Keskenler M., Dal, D., Aydın, T., "Yapay Zeka Destekli ÇOKS Yöntemi ile Kredi Kartı Sahtekarlığının Tespiti", *El-Cezeri Journal of Science and Engineering*, 2021, 8(2):1007-1023.
- [15]. Aylak B., Oral O., Yazıcı K., "Yapay Zeka ve Makine Öğrenmesi Tekniklerinin Lojistik Sektöründe Kullanımı", *El-Cezeri Journal of Science and Engineering*, 2021, 8(1):74-93.
- [16]. Çınar S., Bünyan Ünel F., "2/B orman vasfını yitirmiş araziden tarım arazisine dönüşen taşınmazların toplu değerlendirilmesi", *Geomatik*, 2022, 7(2): 112-127.
- [17]. Demiryeye İ., Ulukavak M., "Derin öğrenme tabanlı iyonosferik TEC tahmini", *Geomatik*, 2022, 7(2): 80-87.
- [18]. Öztürk A., Allahverdi N., Saday F., "Application of artificial intelligence methods for bovine gender prediction", *Turkish Journal of Engineering*, 2022, 6(1): 54-62.
- [19]. Sertkaya C., Akçay S., "Giysi Endüstrisinde Üretim Performansının Tahmininde Yapay Sinir Ağlarının Kullanılması", *Avrupa Bilim ve Teknoloji Dergisi*, 2021, (28): 34-39.
- [20]. Gemirter. C. B., Goularas D., "A Turkish Question Answering System Based on Deep Learning Neural Networks", *Journal of Intelligent Systems: Theory and Applications*, 2021 4(2): 65-75.
- [21]. Darendeli B. N., Yılmaz A., "Convolutional Neural Network Approach to Predict Tumor Samples Using Gene Expression Data", *Journal of Intelligent Systems: Theory and Applications*, 2021, 4(2): 136-141.
- [22]. Kamber E., Körpüz S., Can M., Yumurtacı Aydoğmuş H., Gümüş M., "Yapay Sinir Ağlarına Dayalı Kısa Dönemli Elektrik Yüğü Tahmini", *Endüstri Mühendisliği*, 2021, 32 (2):364-379.
- [23]. Grieder P.K.F., "Cosmic Rays at Earth", 1st ed., Elsevier Science, Amsterdam (2001).
- [24]. Hohlmann M., Ford P., Gnanvo K., Helsby J., Pena D., Hoch R., et al., "GEANT4 simulation of a cosmic ray muon tomography system with micropattern gas detectors for the detection of High Z materials", *IEEE Trans. Nucle. Sci.*, 2009, 56(3):1356-1363.

- [25]. Priedhorsky W.C., Borozdin K.N., Hogan G.E., Morris C., Saunders A., Schultz L.J. et al., "Detection of high-Z objects using multiple scattering of cosmic ray muons", *Review of Scientific Instruments*, 2003, 74:4294.
- [26]. Schultz L.J., Borozdin K.N., Gomez J.J., Hogan G.E., McGill J.A., Morris C.L. et al., "Image reconstruction and material discrimination via cosmic ray muon radiography", *Nuclear Instruments and Methods in Physics Research Section A*, 2004, 519(3):687-694.
- [27]. Schultz J.L., Blanpied G.S., Borozdin K.N., Fraser A.M., Hengartner N.W., Klimenko A.V. et al., "Statistical reconstruction for cosmic ray muon tomography", *IEEE Trans. Image Process*, 2007, 16(8):1985-1993.
- [28]. Jin Jo W., Kim H., An J.S., Lee Y.C., Baek C., Chung Y.H., "Design of a muon tomography system with a plastic scintillator and wavelength-shifting fiber arrays", *Nuclear Instruments and Methods in Physics Research Section A*, 2013, 732:568-572.
- [29]. Roberts T.J., Beard K.B., Huang D., Ahmed S., Kaplan D.M., Spentzouris L.K., "G4Beamline Particle Tracking in Matter-dominated Beam Lines", 11th European Conference, EPAC, 2008, Genoa. C 0806233, WEPP120.
- [30]. Agostinelli S., Allison J., Amako K., Apostolakis J., Araujo H., Arce P. et al., "Geant4—a simulation toolkit", *Nuclear Instruments and Methods in Physics Research Section A*, 2003, 506(3):250-303.
- [31]. Allison J., Amako K., Apostolakis J., Araujo H., Arce P., Asai M. et al., "Geant4 developments and applications", *IEEE Transactions on Nuclear Science*, 2006, 53(1):270-278.
- [32]. Allison J., Amako K., Apostolakis J., Arce P., Asai M., Aso T. et al., "Recent developments in Geant4", *Nuclear Instruments and Methods in Physics Research Section A*, 2016, 835:186-225.
- [33]. Keras, (2021). <https://keras.io>. (Accessed 15 March 2021).
- [34]. Tensorflow, (20121). <https://www.tensorflow.org>. (Accessed 15 March 2021).
- [35]. Glorot X., Bordes A., Bengio Y., "Deep Sparse Rectifier Neural Networks", *Proceedings of the Fourteenth International Conference on Artificial Intelligence and Statistics*, PMLR, 2011, Fort Lauderdale, 15:315-323.
- [36]. Kingma D.P., Ba J., "Adam: A Method for Stochastic Optimization", arXiv:1412.6980v9 [cs.LG], 2017.
- [37]. Deng L., Li J., Huang J.T., Yao K., Yu D., Seide F. et al., "Recent advances in deep learning for speech research at Microsoft", *IEEE International Conference on Acoustics, Speech and Signal Processing, ICASSP*, 2013, Vancouver: IEEE, 13859384.
- [38]. Krizhevsky A., Sutskever I., Hinton G.E., "Imagenet classification with deep convolutional neural networks", *Communications of the ACM*, 2017, 60(6):84-90.
- [39]. Hinton G.E., Salakhutdinov R.R., "Reducing the dimensionality of data with neural network", *Science*, 2006, 313 (5786):504-507.
- [40]. Hinton G., Deng L., Yu D., Dahl G.E., Mohamed A., Jaitly N. et al., "Deep neural networks for acoustic modeling in speech recognition: The shared views of four research groups", *Signal Processing Magazine, IEEE*, 2012, 29(6):82-97.
- [41]. Graves A., Mohamed A., Hinton G., "Speech recognition with deep recurrent neural networks", *International Conference on Acoustics, Speech and Signal Processing, ICASSP*, 2013, Vancouver: IEEE, pp. 6645-6649.
- [42]. Duchi J., Hazan E., Singer Y., "Adaptive subgradient methods for online learning and stochastic optimization", *The Journal of Machine Learning Research*, 2011, 12:2121-2159.
- [43]. Tieleman T., Hinton G., "Lecture 6.5-rmsprop: Divide the gradient by a running average of its recent magnitude", *COURSERA: Neural Networks for Machine Learning*, 2012, 4(2):26-31.